

$E1$ Transitions from the Y'' State and the Fine Structure of the χ'_b States

M. Narain, D. M. J. Lovelock, U. Heintz, J. Lee-Franzini, R. D. Schamberger, J. Willins,
and C. Yanagisawa

State University of New York at Stony Brook, Stony Brook, New York 11794

P. Franzini, P. M. Tuts, S. Kanekal, and Q. W. Wu

Columbia University, New York, New York 10027

(Received 14 January 1991)

Using the CUSB-II detector at the Cornell Electron Storage Ring, we have made precision measurements of the electric dipole transition rates from Y'' to χ'_b , which are in excellent agreement with theory. The fine-structure splitting is found to be $M(\chi'_{b2}) - M(\chi'_{b1}) = 13.5 \pm 0.4 \pm 0.5$ MeV and $M(\chi'_{b1}) - M(\chi'_{b0}) = 23.2 \pm 0.7 \pm 0.7$ MeV, leading to a ratio $R = 0.584 \pm 0.024 \pm 0.02$. The fine structure measures the relative contributions of the spin-orbit interaction $a = 9.5 \pm 0.2 \pm 0.1$ MeV and tensor interaction $b = 2.3 \pm 0.1 \pm 0.1$ MeV. We also find that the long-range confining potential transforms as a Lorentz scalar.

PACS numbers: 14.40.Gx, 12.40.Qq, 13.40.Hq

We have used the CUSB-II detector at the Cornell Electron Storage Ring (CESR) to study the electric dipole ($E1$) transitions in the $b\bar{b}$ system. Triplet S -wave $b\bar{b}$ states, Y 's, are resonantly produced in e^+e^- collisions, whereas triplet P -wave $b\bar{b}$ states, χ_b 's, are reached via the $E1$ transition $Y \rightarrow \chi_b + \gamma$. The fine structure of the χ_b states provides information about the spin dependence of the interquark forces and the Lorentz transformation properties of the confining potential. In this paper we present a precision measurement of the fine structure of the χ'_b from a study of the "inclusive" photon spectrum due to the process $Y'' \rightarrow \gamma + \text{hadrons}$.

The CUSB-II detector consists of a bismuth germanate (BGO) calorimeter, surrounded by an array of NaI and Pb-glass blocks, and covers a solid angle of $\sim 66\%$ of 4π . A drift chamber (DC) between the beam pipe and the BGO cylinder provides charged-particle tracking. The detector has been described in detail elsewhere.¹ We calibrate the calorimeter during data taking with sources embedded between crystal layers. The rms energy resolution is measured to be 0.98% for 5-GeV electrons from Bhabha scatterings.

The Y states that lie below the threshold for open b -flavor production predominantly annihilate into $g\bar{g}$ or a virtual photon which decays into a $q\bar{q}$ or lepton pair; the $g\bar{g}$ and $q\bar{q}$ subsequently hadronize. In addition, the higher excited states can decay via $E1$ transitions to the lower-lying χ_b states with rates comparable to the annihilation rates. They can also decay to lower Y states via hadronic transitions. The χ_b states can in turn decay radiatively to lower-lying Y states, or to D states, $Y(1D)$, which are predicted to exist.² They can also annihilate into $g\bar{g}$ for spin $J=0,2$ states and $gq\bar{q}$ for the $J=1$ state. The bound states Y , Y' , and Y'' have masses of 9.460, 10.023, and 10.355 GeV, respectively. At the Y'' resonance, a significant fraction (46%) of the observed ha-

dronic events are produced by the continuum process $e^+e^- \rightarrow q\bar{q}$. Thus, the data presented here, which consist of 1.6×10^6 hadronic events, correspond to 9.9×10^5 produced Y'' resonance events, obtained from an integrated luminosity of 217.3 pb^{-1} .

A typical hadronic event, at the Y'' energy, has an observed multiplicity of ten isolated energy clusters and deposits an average of 3.5 GeV in the BGO. Therefore, the trigger requires a minimum of 800 MeV in the BGO. A hadronic event is recognized by the presence of tracks with constant dE/dx in the calorimeter due to the passage of fast charged hadrons. The segmentation of the calorimeter is utilized to distinguish between electromagnetic (EM) showers, hadronic showers, and tracks. To identify a photon, we require that the energy deposition pattern in BGO be consistent with an EM shower profile and that there be no DC tracks within $\pm 5^\circ$ of the shower. The photon search code used emphasizes searches for the rarer EM transitions, thus maximizing the photon finding efficiency at the cost of resolution. The detector response is obtained by adding Monte Carlo (MC) -generated monochromatic photons to real hadronic events. The resolution function³ is parametrized as a Gaussian with a low-energy tail due to energy leakage out of the sides of the calorimeter and artifacts of the clustering algorithm. The shape of this function is energy independent, while the fractional resolution scales as $1/E^{1/4}$. In particular, σ of the Gaussian varies versus its peak position E as $\sigma/E = \kappa/[E(\text{GeV})]^{1/4}$, with $\kappa = (3.1 \pm 0.2)\%$, for energies between 70 MeV and 1 GeV.

The inclusive photon spectrum obtained at the Y'' energy is shown in Fig. 1, plotted in 3% energy bins. Signals from the $E1$ decays appear as distinct narrow structures above a large smooth background. The background is mainly due to photons from decays of π^0 's pro-

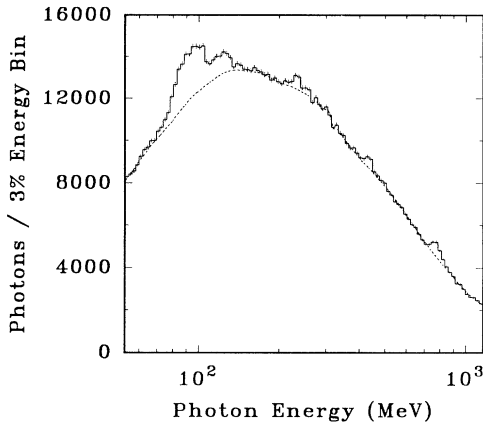


FIG. 1. Inclusive photon spectrum at the Y'' peak. The dashed curve represents background.

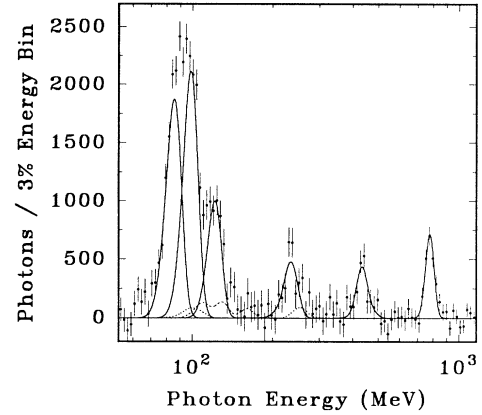


FIG. 2. Background-subtracted photon spectrum. The curves are described in the text.

duced in the hadronization of gluon and quark final states. We characterize event topologies by thrust⁴ and multiplicity. Decays into ggg give lower thrust and higher multiplicity than those with gg or $q\bar{q}$. We predict the background shape and absolute normalization by combining the photon spectra obtained from 41.4 pb^{-1} of data taken at the $Y(1S)$ resonance and 210.5 pb^{-1} from continuum running. Relative proportions of $Y(1S)$ and continuum hadronic events are combined according to luminosity, resonance production cross sections, and decay ratios with minute adjustments of the order of 1%,⁵ so that the values of global variables (thrust, multiplicity, average energy) for the combined distribution reproduce those of the Y'' data. A minor rescaling of the spectra is also performed. The background is shown as a dashed curve in Fig. 1 and includes a $\sim 3\%$ contribution from the hadronic transitions $Y'' \rightarrow \pi^0 \pi^0 Y'(\gamma)$, which are modeled by adding MC-generated π^0 's to hadronic events from $Y(1S)$ data. Figure 2 shows the background-subtracted photon spectrum.

The solid curves in Fig. 2 are a fit to the data, allowing for all expected $E1$ transitions, using the resolution function mentioned above. The energies and intensities of these transitions are free parameters of the fit. The χ^2/N_{DF} for the fit is 0.99. The first three prominent lines, at $E_\gamma \approx 85\text{--}125 \text{ MeV}$, correspond to the transitions $Y'' \rightarrow \chi'_{bJ} \gamma$. The first two signals, $J=2$ and 1, are just resolved while the third, $J=0$, is well resolved. The values for the energies of these three lines given in Table I are in excellent agreement with the energies measured by an analysis of the "exclusive" decays⁶ in which the first two lines are completely resolved. The systematic error on the energy scale due to combined effect of calibration uncertainty as obtained in Ref. 6 and dependence of peak positions on the photon selection criterion is determined to be 0.9%. From the measured photon energies, we obtain the center of gravity of the χ'_b states $\bar{M} = 10259.7 \pm 0.4 \pm 1.0 \text{ MeV}$. The peak at $\sim 230 \text{ MeV}$

is due to the transitions $\chi'_{bJ} \rightarrow Y' \gamma$ and the peak at $\sim 760 \text{ MeV}$ originates from the decay $\chi'_{bJ} \rightarrow Y \gamma$. For these transitions from the χ'_{bJ} to the lower Y states, the $J=2, 1, 0$ components are not resolved. Table I lists the fitted values for the energies and the number of photons.

The peak at $\sim 450 \text{ MeV}$ is a superposition of the transitions $Y'' \rightarrow \chi_{bJ} \gamma$ and $\chi_{bJ} \rightarrow Y \gamma$. The signal $\chi_{bJ} \rightarrow Y \gamma$ is enhanced by the process $Y' \rightarrow \chi_b \gamma$, shown as dashed curves around $\sim 100\text{--}160 \text{ MeV}$ and fixed to previously measured values.⁷ The Y' is reached from the Y'' via radiative and hadronic transitions. The $E1$ transitions to χ_b via the $Y(1D)$ states are shown as dotted curves at 100 and 230 MeV and are fixed to predicted² values. Their observation is hindered by much stronger transitions. The data are consistent with the predictions, for which χ^2 has a shallow minimum and increases by 0.7 without D -state production.

In order to determine acceptance \times efficiency (ϵ) for finding a photon, MC-generated monochromatic photons are added to real hadronic events to simulate the decay chain. χ'_{bJ} hadronic decays are simulated by adding MC photons to continuum data which consist of $q\bar{q}$ final states. To model Y decays we add MC photons to $Y(1S)$ data and statistically subtract the continuum contribution. For the Y'' decays to the χ'_{bJ} the values of ϵ are 0.105, 0.111, and 0.095 for $J=2, 1$, and 0, respectively, and are determined to 4% of their value.⁸ The efficiencies for the χ'_b decays to the Y' and Y are 0.065 and

TABLE I. Branching ratios (BR) of transitions from Y'' .

Transition	E_γ (MeV)	Events	BR (%)
$Y'' \rightarrow \chi'_{b2} \gamma$	86.7 ± 0.4	10319 ± 478	$11.1 \pm 0.5 \pm 0.4$
$Y'' \rightarrow \chi'_{b1} \gamma$	100.1 ± 0.4	11147 ± 462	$11.5 \pm 0.5 \pm 0.5$
$Y'' \rightarrow \chi'_{b0} \gamma$	123.0 ± 0.8	4959 ± 339	$6.0 \pm 0.4 \pm 0.6$
$\chi'_{bJ} \rightarrow Y' \gamma$	236.1 ± 2.6	2429 ± 332	$4.2 \pm 0.6 \pm 0.5^\dagger$
$\chi'_{bJ} \rightarrow Y \gamma$	770.3 ± 2.9	1994 ± 150	$2.0 \pm 0.2 \pm 0.2^\dagger$

TABLE II. $E1$ rates for $Y'' \rightarrow \chi'_{bJ} + \gamma$ in keV.

J	Experiment	GRR	MR	MB	KR	PF	LF
2	$2.7 \pm 0.1 \pm 0.3$	2.6	3.0	2.8	2.8	2.8	2.7
1	$2.8 \pm 0.1 \pm 0.4$	2.4	2.6	2.2	2.6	2.6	2.5
0	$1.5 \pm 0.1 \pm 0.2$	1.5	1.5	1.0	1.6	1.6	1.6
Σ	$7.0 \pm 0.2 \pm 0.5$	6.5	7.1	6.0	7.0	7.0	6.8

0.11, respectively, and 0.15 for Y'' to χ_b , determined to 10% of their value. Errors on the efficiencies are mainly due to uncertainties in the Monte Carlo modeling of the decay chain. From the fitted number of photons and ϵ we obtain the branching ratios listed in Table I. The first error is statistical and the second is systematic. The numbers marked with a dagger are the measured product branching ratios $\sum_J B(Y'' \rightarrow \chi'_{bJ} \gamma) B(\chi'_{bJ} \rightarrow Y(Y') \gamma)$. They agree with the rates measured by the exclusive analysis.

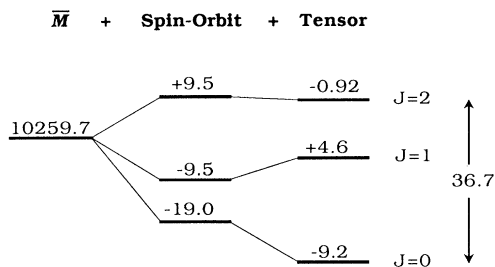
Using the total width of the Y'' of 24.3 ± 2.9 keV,⁷ we derive the rates (Γ_{E1}) of the $E1$ transitions $Y'' \rightarrow \chi'_{bJ} \gamma$. In Table II we compare the measured rates with predictions of the relativistic models of Gupta, Radford, and Repko (GRR),⁹ Moxhay and Rosner (MR),¹⁰ and McClary and Byers (MB),¹¹ the inverse scattering potential of Kwong and Rosner (KR),² and the Richardson potential with parameters adjusted by Franzini¹² (PF) and Fulcher (LF).¹³ The predicted rates are computed using the observed photon energies E_γ and the $E1$ matrix element $\langle r \rangle$ given by potential models: $\Gamma_{E1} \propto (2J+1)E_\gamma^3 |\langle r \rangle|^2$. Our measured rates are accurate to 5% of their values, a factor of 6 better than previously published values.¹⁴ The agreement between experiment and theory is excellent, indicating the success of potential-model builders in describing the features of the central potential.

The fitted area of the 450-MeV signal together with the previously measured⁷ branching ratios of $Y'' \rightarrow Y' + X$, $Y' \rightarrow \chi_b \gamma$, and $\chi_b \rightarrow Y \gamma$ leads to the product branching ratio

$$\sum_J B(Y'' \rightarrow \chi'_{bJ} \gamma) B(\chi'_{bJ} \rightarrow Y \gamma) = (1.7 \pm 0.4 \pm 0.6) \times 10^{-3}.$$

The $E1$ rates for the process $Y'' \rightarrow \chi'_{bJ} \gamma$ are extremely sensitive to details of the potential, owing to the different numbers of nodes in the radial wave functions of the initial and final states.¹¹ There are a range of predictions for this product branching ratio; the Cornell model estimates 10.2×10^{-3} ,¹⁵ while the above-mentioned models predict between 0.5×10^{-3} and 1.8×10^{-3} . Our data favor the upper end of this range given by the relativistic models of GRR and MR.

We have also searched for the singlet S state η_b in the cascade $Y'' \rightarrow \pi \pi h_b \rightarrow \pi \pi \gamma \eta_b$, which is expected to have a product branching ratio of about (0.05–0.5)%.¹⁶ The transition from the singlet P state h_b to η_b is signaled by a monochromatic photon of about 480 MeV. We fix the

FIG. 3. Fine structure of the χ'_b states. Energies are in MeV.

energy and branching ratio and determine our sensitivity by varying them for a unit change in χ^2 while leaving other parameters free. We find that the product branching ratio $B(Y'' \rightarrow \pi \pi h_b) B(h_b \rightarrow \gamma \eta_b) < 0.45\%$ (90% C.L.) for an Y - η_b splitting between 50 and 110 MeV.¹⁷

We shall now examine the character of the spin-dependent forces. The fine structure of the χ'_b states varies from the spin-orbit and the tensor forces of the interquark potential. In general, the interquark potential is comprised of a scalar component S and a vector component V . The χ'_b masses are given by $M(\chi'_{b2}) = \bar{M} + a - 2b/5$, $M(\chi'_{b1}) = \bar{M} - a + 2b$, $M(\chi'_{b0}) = \bar{M} - 2a - 4b$, where a and b are expectation values of spin-orbit and tensor interactions: $a = \langle 3V'/r - S'/r \rangle / 2M_Q^2$, $b = \langle V'/r - V'' \rangle / 12M_Q^2$.¹⁸ From Table I we find the level splittings to be $M(\chi'_{b2}) - M(\chi'_{b1}) = 13.5 \pm 0.4 \pm 0.5$ MeV, $M(\chi'_{b1}) - M(\chi'_{b0}) = 23.2 \pm 0.7 \pm 0.7$ MeV, and $M(\chi'_{b2}) - M(\chi'_{b0}) = 36.7 \pm 0.8 \pm 0.9$ MeV, as shown schematically in Fig. 3. In Table III, we compare our measurement of a and b to theoretical models, which differ in their assumptions of V and S . The data confirm the dominance of the spin-orbit force over the tensor force, a common feature of all the models, but the absolute value disagrees most with the predictions of MR and MB.

A concise way to describe the fine structure is the ratio

$$R = [M(\chi'_{b2}) - M(\chi'_{b1})] / [M(\chi'_{b1}) - M(\chi'_{b0})].$$

In the lower half of Table III we list our measurement of R for χ'_b together with values of R for χ'_c and χ'_b .⁷ With our precise $R(\chi'_b)$ value, there is an indication that

TABLE III. Spin-orbit and tensor contributions to the χ'_b fine structure and the ratio R .

	Experiment	GRR	MR	MB	PF	LF
a (MeV)	$9.5 \pm 0.2 \pm 0.2$	9.3	6.5	14.6	8.3	10.3
b (MeV)	$2.3 \pm 0.1 \pm 0.1$	1.9	2.1	4.2	1.6	1.9
$R(\chi'_c)$	0.48 ± 0.01	0.50	0.42	0.35		0.56
$R(\chi'_b)$	0.66 ± 0.05	0.64	0.42	0.45	0.70	0.67
$R(\chi'_b)$	$0.584 \pm 0.024 \pm 0.02$	0.67	0.42	0.48	0.71	0.70

$R(\chi'_b)$ is smaller than $R(\chi_b)$, contrary to all model expectations.¹⁹ Therefore, an improvement in the determination of $R(\chi_b)$ would help resolve this apparent discrepancy. Alternatively, this effect can be explained by the possibility of mixing between the $\chi'_{bJ=2}$ and $1^3F_{J=2}$ states due to an additional tensor interaction.¹² The as yet unobserved 3F_J states are expected by potential models to lie close to the χ'_b . PF calculates the amount of mixing as a function of the mass difference $\Delta M = M(1^3F) - M(\chi'_b)$. Expressed in terms of the off-diagonal term in the mass-squared mixing matrix, scaled by the diagonal terms, a very small amount of mixing ranging between 0.04% and 0.4% for ΔM varying between 0 and 200 MeV is required by our observation.

A Coulomb potential, $-4\alpha_s/3r$, gives $R=0.8$. The addition of a linear, scalar term (kr) decreases its value.¹⁹ We can use our measured value of R to estimate the fraction (f) of the long-range term transforming as a scalar, by parametrizing the vector and scalar $q\bar{q}$ potential as $V(r) = -4\alpha_s/3r + (1-f)kr$, $S(r) = fkr$. We express f in terms of R and the static potential parameter $\lambda = (k/\alpha_s)(\langle r^{-1} \rangle / \langle r^{-3} \rangle)$.³ We calculate f for values of k/α_s in the range 0.5–1.5, favored by potential models, and use $\langle r^{-1} \rangle / \langle r^{-3} \rangle = 1.2$ for χ_b and 1.1 for χ'_b .^{2,12} The values of f obtained for χ_b and χ'_b differ by about 1.5σ and the weighted average varies between 0.9 and 1.3, consistent with $f=1$. The statistical error is about 3%. Thus we conclude that the confining potential transforms as a Lorentz scalar.

We wish to thank Paula Franzini for valuable discussions. We also thank the CESR operating staff. This research is supported by the U.S. National Science Foundation.

¹J. Lee-Franzini, Nucl. Instrum. Methods Phys. Res., Sect. A **263**, 35 (1988); P. M. Tuts, Nucl. Instrum. Methods Phys. Res., Sect. A **265**, 243 (1988).

²W. Kwong and J. L. Rosner, Phys. Rev. D **38**, 279 (1988).

³D. M. J. Lovelock, Ph.D. thesis, State University of New York at Stony Brook, 1990 (unpublished).

⁴CUSB Collaboration, D. Peterson *et al.*, Phys. Lett. **114B**, 277 (1982).

⁵Ten-times-bigger adjustments change our final results by a small fraction of the quoted systematic error.

⁶U. Heintz *et al.*, Phys. Rev. Lett. **66**, 1563 (1991).

⁷Particle Data Group, J. J. Hernandez *et al.*, Phys. Lett. B **239**, 1 (1990).

⁸Angular distributions for the MC photons used are those computed by L. S. Brown and R. Cahn, Phys. Rev. D **13**, 1195 (1976).

⁹S. N. Gupta, S. F. Radford, and W. W. Repko, Phys. Rev. D **34**, 201 (1986).

¹⁰P. Moxhay and J. L. Rosner, Phys. Rev. D **28**, 1132 (1983).

¹¹R. McClary and N. Byers, Phys. Rev. D **28**, 1692 (1983).

¹²Paula Franzini, LBL Report No. LBL-30440, 1991 (to be published).

¹³L. P. Fulcher, Phys. Rev. D **39**, 295 (1989).

¹⁴K. Han *et al.*, Phys. Rev. Lett. **49**, 1612 (1982); G. Eigen *et al.*, Phys. Rev. Lett. **49**, 1616 (1982).

¹⁵E. Eichten *et al.*, Phys. Rev. D **17**, 3090 (1978); **21**, 203 (1980).

¹⁶Y. P. Kuang and T. M. Yan, Phys. Rev. D **24**, 2874 (1981); M. B. Voloshin, Yad. Fiz. **43**, 1571 (1986) [Sov. J. Nucl. Phys. **43**, 1011 (1986)].

¹⁷J. Pantaleone, S.-H. H. Tye, and Y. J. Ng, Phys. Rev. D **33**, 777 (1986).

¹⁸J. L. Rosner, in *Experimental Meson Spectroscopy—1983*, edited by S. J. Lindenbaum (AIP, New York, 1984), p. 461.

¹⁹C. O. Dib, F. J. Gilman, and P. J. Franzini, Phys. Rev. D **37**, 735 (1988).